DOI: 10.35840/2631-5033/1867

VIBGYOR ePress

International Journal of
Earth Science and Geophysics

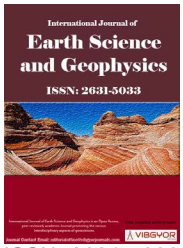

ISSN: 2631-5033

Formation of Oxide and Silicate Nickel Laterites using Reactive Transport Simulations

***Ifeoma M Ugwu*[1,2*] *and Davidson E Egirani*[2]**

[1]*Department of Geology and Mining, Enugu State University of Science and Technology, Agbani, Nigeria*

[2]*Niger Delta University, Wilberforce Island, Nigeria*

Abstract

Geochemical modelling of ore deposit gives preliminary information on the supergene enrichment of the metallic ore in the subsurface. With recent advances in analytical technology, thermodynamic data necessary for modelling rock-mineral weathering and water-mineral interaction have become available, thus enabling the prediction of geochemical processes. The PHREEQC code enables the simulation of weathering, secondary mineral formation, and metal transport using thermodynamic models for mineral dissolution and metal sorption. In Ni laterite deposits, goethite is the host mineral in the oxide type whereas both goethite and garnierite are the host minerals in the silicate type. In both types of Ni laterite, nickel and cobalt are associated with goethite via surface precipitates or surface complexes or by structural incorporation. This study presents a reactive transport simulation for the formation of both silicate and oxic Ni laterite weathering at ambient conditions using PHREEQC with a supplemental thermodynamic model. The PHREEQC simulation of Falcondo Ni laterite (silicate) revealed that the increasing trends of evolution of minerals are goethite, antigorite, sepiolite, falcondoite and enstatite. Similarly goethite, antigorite, enstatite and talc were reproduced for the Koniambo Ni laterites (oxic). For both laterite types, the pH at the limonite zone varies from 9.1 to 8.9; whereas the pH at the saprolite zone is 7.8 (for silicate laterite) and 8.3 (for oxic laterite). Starting from ultramafic rock consisting of forsterite with a mole fraction of 0.827, fayalite (0.1667) and Ni_2SiO_4 (0.006) co-existing as an ideal solid solution, the simulation of the oxic laterite show that 0.28 wt.% Co and 1.18 wt.% of Ni were sorbed on goethite. In contrast, 0.25 wt.% Co and 1.25 wt.% Ni were adsorbed on goethite for silicate Ni laterite simulation. The simulations produce a weathering profile, mineral assemblages and ore grade similar to that observed in natural Ni laterite deposits.

Keywords

Ni Laterite, PHREEQC, Nickel, Goethite, Garnierite

Introduction

The majority of Ni and Co used in manufacturing both super alloys and petrochemicals and in the aviation industry are obtained from Ni laterite deposits [1]. Consequently, the evolution, weathering profile, mineralogy and mode of occurrences of the alteration minerals present in both oxide and silicate types of Ni laterite have been studied by many researchers [2-8]. Goethite is the host mineral in the oxide type whereas both goethite and garnierite are the host minerals in the silicate type [5,6].

***Corresponding author:** *Ifeoma M Ugwu, Department of Geology and Mining, Enugu State University of Science and Technology, Agbani, Nigeria*

Accepted: April 01, 2023; **Published:** April 03, 2023

Citation: Ugwu IM, Egirani DE (2023) Formation of Oxide and Silicate Nickel Laterites using Reactive Transport Simulations. Int J Earth Sci Geophys 9:067

Reactive transport simulations, based on thermodynamics and mass transfer, can be used to investigate weathering processes, regolith formation, weathering profile thickness and metal leaching [9-21]. The PHREEQC (pH-REdox-Equilibrium Code) enables us to simulate weathering, secondary mineral formation, and metal transport using thermodynamic models for mineral dissolution and metal sorption [22]. However, previous attempts to simulate the formation of Ni laterite weathering using PHREEQC were unsuccessful, resulting in an unrealistic pH in the limonite zone containing goethite and variations between the hypothetical and actual layer thickness [17]. In particular, the pH above 7 required for total adsorption of Ni onto goethite was not attained in the previous published models [17,18]. Recent modelling of ultrabasic accounted for Ni adsorption on goethite as well as existence of Ni in the goethite structure and its occurrence as surface complex and precipitates [18]. However, the modelling was done using thermodynamic data obtained for ferrihydrite rather than goethite and unable to explain the Ni enrichment in present day laterites as well as unrealistic high amount of nickel. In addition, no model has been able to account for reproduction of cobalt adsorbed or incorporated in goethite present in Ni laterites Crucial to success of a reactive transport simulation is the thermodynamic (and potentially kinetic) model is it based on.

In the present work, a reactive transport modelling inclusive PHREEQC and the basic Stern model for electrostatics have been used to develop the secondary nickel ores profile with vertical progression of the alteration front. Also, the resulting thermodynamic and PHREEQC models have been used for the advective transport simulation of oxide and silicate laterites as applied for the sorption of Co and Ni by goethite [23,24]. The thermodynamic models used with PHREEQC with equilibrium constants have been used to simulate the precipitation of relevant secondary phases from [25]. The model inputs include those for garnierite (silicate) Ni laterite and limonite (oxide) Ni laterite. The outcome of the modelling provides an in-depth empathy of the weathering mechanism in the Nickel laterites. The validity of the model provides new insights into further processes that control the mobility of elements and formation of these Nickel laterites.

Method

PHREEQC Geochemical modelling of Ni Laterite Formation

The thermodynamic calculations involved the modelling of the Ni laterite formation from weathering of ultramafic rocks were carried out using the geochemical code PHREEQC. This program is well known for its capability for calculating complex sorption reactions between aqueous species and mineral assemblages both in 1D advection-diffusion-reaction and transport mode. Goethite associates with Ni and Co through surface complexation, surface precipitation and structural incorporation; however, existing thermodynamic models (e.g., llnl.dat) available with PHREEQC do have equilibrium constants for surface complexation or structural incorporation. Consequently, we supplemented the existing llnl.dat thermodynamic model with a surface complexation model derived from fitting to laboratory sorption experiments for Ni sorption up to 0.42 wt.% and 0.2 wt.% Co [23,24]. A two-site model was used to describe the surface complexes; the goethite surface area was assumed to be 50.4 m^2g^{-1}. The surface electrostatics was evaluated using a basic Stern layer model with a capacitance of the Stern layer set to 1.05 F/m^2 with all charges at the 0-plane [26]. The surface complexation model is summarised in Table 1.

A number of important secondary phases associated with silicate laterites are not included in the distributed llnl.dat model ("database"). The chemical reactions, equilibrium constants and enthalpy of formation for dominant mineral phases in silicate Ni laterite were obtained from literature [25]. These are reproduced in Table 1. Thus, the llnl.dat thermodynamic model was modified to include thermodynamic parameters for népouite, falcondoite, kerolite and pimelite phases given by [25]. The resulting thermodynamic model was to simulate the formation of oxide Ni laterites (e.g., Koniambo, New Caledonia, Figure 1) [5] and silicate Ni laterites (e.g., Falcondo, Dominican Republic, Figure 2) [3,4].

Model Input: Garnierite (Silicate) Ni Laterite

The parent rocks for the Falcondo Ni laterite are serpentinised peridotite, predominantly harzburgite with minor quantities of lherzolite, dunite and serpentinite [3,7]. The olivine in these rocks contains Fosterite 89 to 92 wt.% and 0.2

Table 1: Dissolution reactions for Mg and Ni end-members of garnierite and Fayalite-Fe, with the corresponding equilibrium constants at 25 °C and 1 bar used for the PHREEQC modelling.

Minerals	Reaction	Log K
Nepouite	$Ni_3Si_2O_5(OH)_4 + 6.00\ H^+ = 3.00\ Ni^{++} + 2.00\ SiO_2 + 5.00\ H_2O$	21.5[a]
Pimelite	$Ni_3Si_4O_{10}(OH)_2{:}H_2O + 6.000\ H^+ = 3.00\ Ni^{++} + 4.00\ SiO_2 + 5.00\ H_2O$	11.46[a]
Falcondoite	$Ni_4Si_6O_{15}(OH)_2{:}6H_2O + 8.0000\ H^+ = +\ 4.0000\ Ni^{++} + 6.0000\ SiO_2 + 11.0000\ H_2O$	12.31[a]
Kerolite	$Mg_3Si_4O_{10}(OH)_2{:}H_2O + 6.000\ H^+ = 3.00\ Mg^{++} + 4.00\ SiO_2 + 5.00\ H_2O$	25.55[a]
Ferrosilite	$FeSiO_3 + 2.0000\ H+ = +\ 1.0000\ Fe^{++} + 1.0000\ H_2O + 1.0000\ SiO_2$	7.447[b]
Enstatite	$MgSiO_3 + 2.0000\ H+ = +\ 1.0000\ H_2O + 1.0000\ Mg^{++} + 1.0000\ SiO_2$	11.3269[b]
Fosterite	$Mg_2SiO_4 + 4.0000\ H+ = +\ 1.0000\ SiO_2 + 2.0000\ H_2O + 2.0000\ Mg^{++}$	27.8626II[b]
Fayalite	$Fe_2SiO_4 + 4.0000\ H+ = +\ 1.0000\ SiO_2 + 2.0000\ Fe^{++} + 2.0000\ H_2O$	19.1113[b]
$Fe(OH)_2Ni$	$>Fe(OH)_2^{-1} + Ni^{2+} = Fe(OH)_2N_i^+$	12.60[c]
$(FeOH)_2Ni$	$2 > FeOH^{-0.5} + Ni^{2+} = (> FeOH)_2Ni^+$	10.1[c]
$Fe(OH)_2Co$	$> Fe(OH)_2^{-1} + Co^{2+} = Fe(OH)_2Co^+$	12.80[d]
$(FeOH)_2Co$	$2 > FeOH^{-0.5} + Co^{2+} = (> FeOH)_2Co^+$	10.60[d]

[a]Gali, et al [25]; [b]LLNL database [29], [c]Ugwu, et al. [24], [d]Ugwu and Sherman [23].

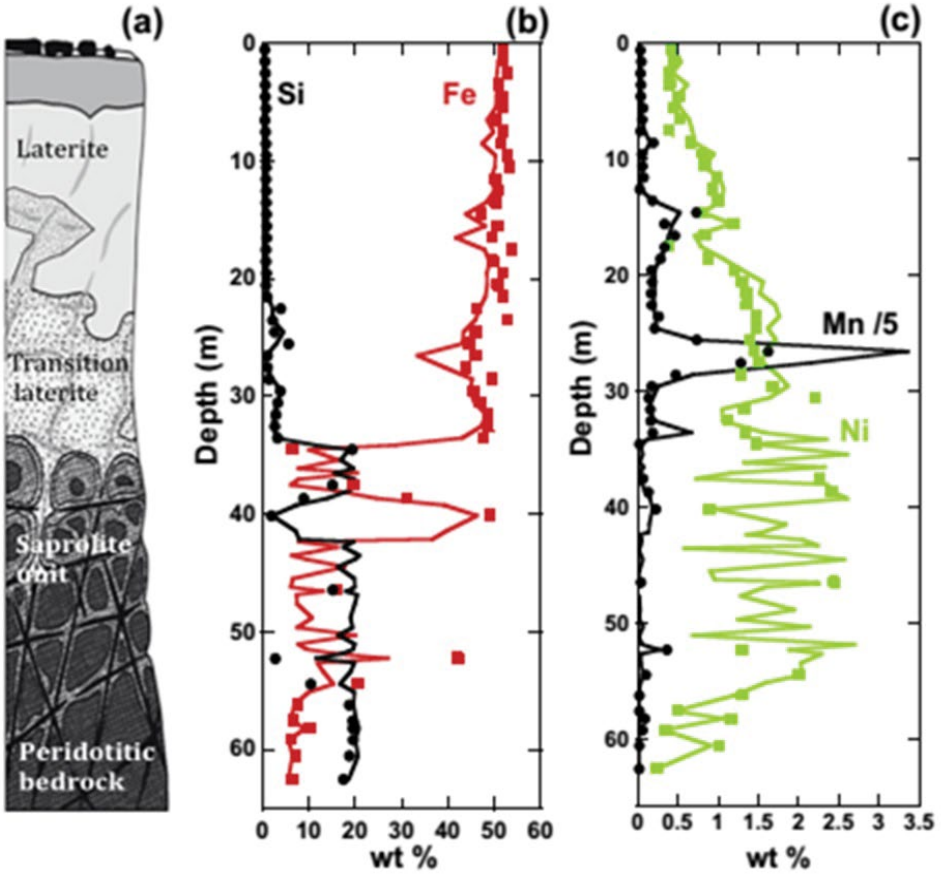

Figure 1: a) Schematic representation of major regolith units of Koniambo Ni laterite deposit; b) Percent weight (wt.%) of Fe and Si and c) Ni and Mn versus depth along the studied profile (Source: Dublet, et al. [5]).

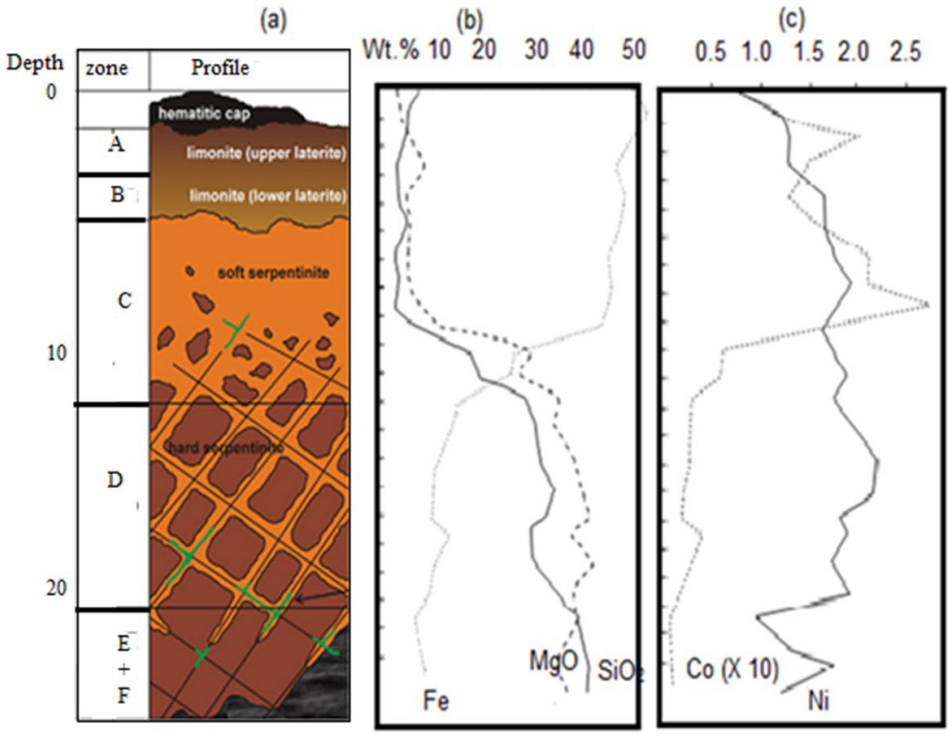

Figure 2: a) Schematic representation of major regolith units of Falcondo Ni laterite deposit Dominican Republic b) Percent weight (wt.%) of Fe, MgO and SiO_2 and c) Ni and Co versus depth along the studied profile (modified from [2-4,7]).

to 0.4 wt.% Ni [27,28]. These rocks weather to form Ni laterite with six distinct layers from top to base, namely: upper limonite, lower limonite, soft serpentine, hard serpentine, serpentinised peridotite and unaltered ultramafic protolith. The thickness of the layers are 0.8 m, 10 m, 13 m, 17 m, 19 m and 23 m from top to base. The secondary minerals identified are Ni-sepiolite-falcondoite, Ni serpentine, goethite, kerolite, pimelite, and lizardite-nepouite [3,7].

Our starting primary mineral assemblage consisted of olivine comprised of forsterite with a mole fraction of 0.827, fayalite (0.1667), Ni_2SiO_4 (0.005) and Co_2SiO_4 (0.001) co-existing as an ideal solid solution. This mole fraction was chosen to represent the composition of serpentinised peridotite described by Lewis, et al. [3]. The silicate laterite simulation was allowed to react with rainwater with pH 5.7 and equilibrate with antigorite, sepiolite, goethite, Ni_2SiO_4, Co_2SiO_4, enstatite, ferrosilite, nepouite, pimelite, falcondoite, kerolite and atmospheric CO_2. The simulation is made up of layers of 6 cells of variable thickness. The detailed input file for this simulation and the results obtained in molality and wt.% are shown in Appendix.

The oxic laterite profile consists of ten layers with different proportions of iron oxides and secondary silicates [5]. The layers are primarily rock containing forsterite with < 0.4 wt.% Ni, enstatite and serpentine. These units have variable thicknesses and an overall thickness of 64m starting from the top unit and finishing at the bedrock. The boundary between limonite and saprolite zones occurs at 34m depth. The minerals present in the profile are goethite, asbolane, serpentine, lithiophorite, forsterite, hematite, talc, quartz, enstatite, chromite and birnessite. Except at the bedrock, goethite occurs throughout the profile [5].

The simulation started with a primary mineral assemblage consisting of olivine comprised of forsterite with a mole fraction of 0.827, fayalite (0.1667), Ni_2SiO_4 (0.006) and Co_2SiO_4 (0.001) co-existing as an ideal solid solution. The simulation was allowed to react with rain water with pH 5.7 and equilibrate with antigorite, sepiolite, goethite, talc, enstatite, birnessite and atmospheric CO_2. The simulation is made up of layers of 10 cells of variable thickness and the no. of shifts used is 120. Therefore, the total number of years for the simulation is 1200 years (no. of cells x shifts). The input file is similar to that of the silicate Ni laterite

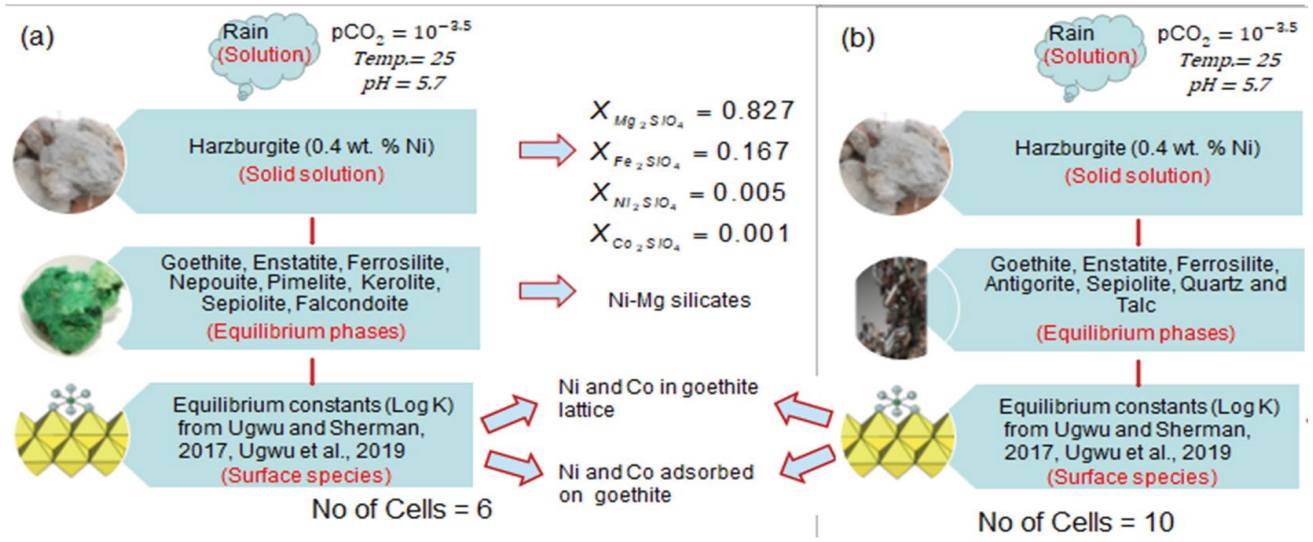

Figure 3: Steps for modelling oxide a) Silicate (Falcondo Ni laterite; b) Oxide (Koniambo) Ni laterite deposit.

expect that minerals that are formed on oxic Ni laterite are allowed to precipitate. The input parameters are illustrated in Figure 3 whereas the input values for the constants are shown in Table 1.

Ordinarily, mineral assemblage of phyllosilicates and Ni are components of solid solution series extending throughout the assemblage- Ni end-members [30]. Their effect is presented as an ideal solid solution instead of separate minerals. Some ground waters derived from the base of nickel laterite profiles are soaked with respect to talc-like mineral but not with serpentine [31]. Serpentine is seldomly form under ambient conditions and curbed from the phases of equilibrium allowed for precipitation. In real-life the rates of precipitation support the development of metastable sepiolite and kerolite in Al-poor environments [32]. The inclusion of nickel as a starter to the assemblage system enhances the stability of the Nepouite phase, thus preventing its development to Fayalite [33]. The surface complexation model of [34], takes in consideration the attachment of metals and protonation on strong and weak reactive sites of a mineral phase (Table 1b). The binding of these metals and subsequent protonation generates a charge on the ions sorbed and has been used to simulate the adsorption process. A charge depending on the ions sorbed, has been used in order to simulate adsorption process.

Results

Reactive transport simulation

The reactive transport simulations replicate the secondary mineralogy of natural silicate (Figure 1) and oxide laterites (Figure 2). The simulation of silicate Ni laterite revealed that the increasing trends of evolution of minerals are goethite, antigorite, sepiolite, falcondoite and enstatite. This is consistent with observation by [3,7,25]. Similarly, in order of increasing succession, the mineral reproduced for oxide laterites are goethite, antigorite, enstatite, talc and Ni_2SiO_4 which is consistent with that observed by [5].

Even though minerals such as pimelite, kerolite and nepouite were allowed to equilibrate, they did not precipitate out of solution. The formation of some secondary mineral phases may be thermodynamically favoured but limited by kinetics of precipitation e.g., birnessite, asbolane, serpentine. However, in the absence of kinetic models for these mineral, the only approach to is to prevent them from forming during the simulation. If the formation of antigorite is suppressed, then kerolite will form instead but prevent the formation of sepiolite and falcondoite with increase in the pH of the saprolite zone from 8.4 to 11.3. In the simulation reported here, however, no phases were suppressed and the resulting mineralogy is in agreement with field observations. For both laterite types, the pH (Figure 4) at the limonite zone varies from 9.1 to 8.9 whereas the pH at the silicate-saprolite zone is 7.8 and the oxide-saprolite zone is 8.3. Also, the pH-depth diagram for silicate-Falcondo Ni laterite in the limonite zone range from pH = 7-9 at a depth of 0-1.5 m and saprolite zone is from pH = 7-8 at a depth of 1.5- 4 m (Figure 4a and Figure 4b).

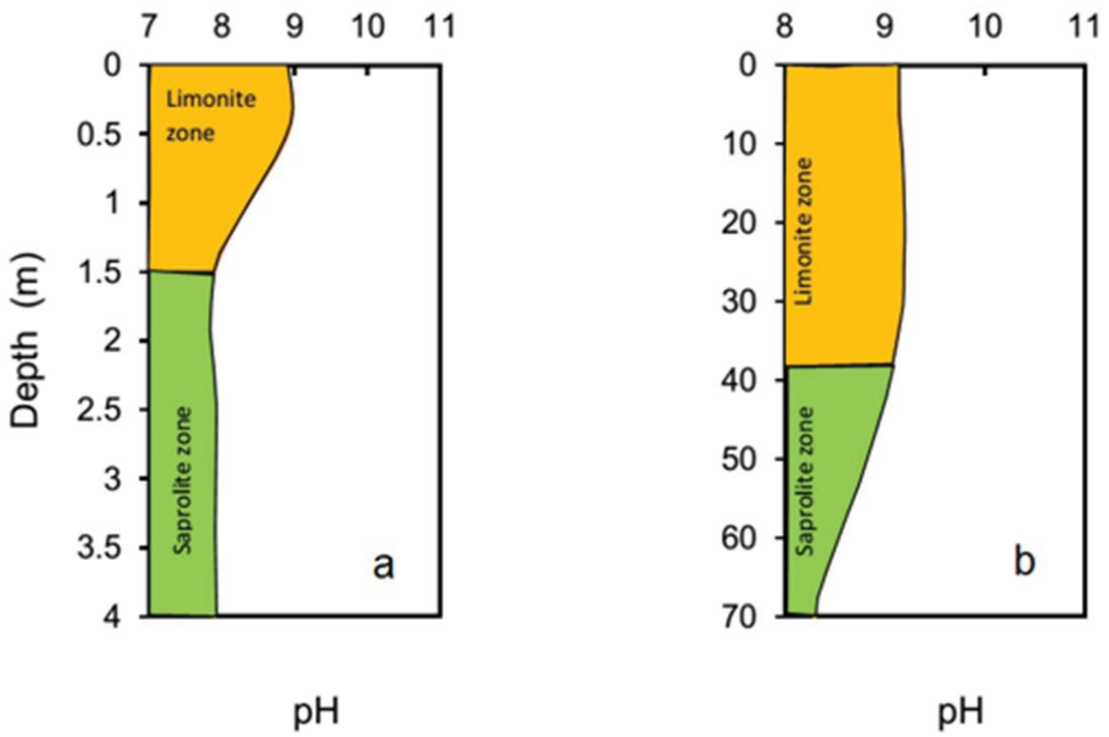

Figure 4: Plots of pH vs. depth for a) Falcondo Ni laterite (silicate) and b) Koniambo Ni laterite (oxic).

This is in agreement with the pH 6.2 to 9.2 in the ferricrete and coarse saprolite zones of natural Ni laterite [35]. Similarly, at Cerro Matoso Ni laterite deposit, pH 8.1 was observed at the spring located at the base of the weathering profile [36]. At pH above 8, garnierite minerals are slightly soluble [7] while all the Ni released sorbs to goethite at pH > 7.

Starting from ultramafic rock with forsterite with a mole fraction of 0.827, fayalite (0.1667) and Ni_2SiO_4 (0.006) co-existing as an ideal solid solution, the simulation of oxic Ni laterite containing both Ni and Co, yielded 0.0001% Co adsorbed at the weak but abundant site (> $(FeOH)_2$), as well as 0.28 wt.% Co at the strong but unabundant site (> $Fe(OH)_2$) of goethite. Similarly, 1.18 wt.% of Ni was adsorbed at the > $(FeOH)_2$ site while 0.003 wt.% Ni was adsorbed at the > $Fe(OH)_2$ site. In contrast, for the silicate Ni laterite containing both Ni and Co, 2.9×10^{-5}% Co was adsorbed on (> $(FeOH)_2$) site of goethite while 0.25 wt.% Co was adsorbed at the > $Fe(OH)_2$ site. Similarly, 1.25 wt.% Ni was adsorbed at the (> $(FeOH)_2$) site while 0.009 wt.% Ni was adsorbed at the > $Fe(OH)_2$ site of goethite. This is consistent with the findings of [5] for transition laterite (0 to 34 m) containing 0.8 to 1.5 wt% Ni and 0.1 to 0.3 wt.% Co although they found 2.44 wt.% Ni and 0.09 wt.% Co at depth of 46.5 m.

Weathering process and the formation of Falcondo Ni laterite, Dominican Republic

The simulation provides a spatial distribution of mineral phases with chemical species present after sorption of Ni and Co on goethite (Figure 5a, Figure 5b and Figure 5c).

Also, secondary mineral phases (i.e. $Fe(OH)_2Ni$), $(FeOH)_2Ni$, $Fe(OH)_2Co$, (FeOH)Co, antigorite, goethite, sepiolite and falcondite. The alteration mineral succession depicts that of natural silicate Ni laterite deposits.

The plot of elements versus depth for the silicate Ni laterite (Figure 6) indicate low amount of Ni, Mg, Fe and Si at the limonite zone as well as high Si, Ni and Mg at the saprolite zone. This trend closely matches that of natural Ni laterite. Magnesium, iron, nickel and silica are main components of the garnierite minerals.

Weathering process and formation of Koniambo Ni laterite, New Caledonia

The simulation provides a spatial distribution of mineral phases with chemical species present after Ni and Co sorption on goethite (Figure 7a, Figure 7b and Figure 7c). The secondary minerals generated include $Fe(OH)_2Ni$, $(FeOH)_2Ni$, $Fe(OH)_2Co$, (FeOH)

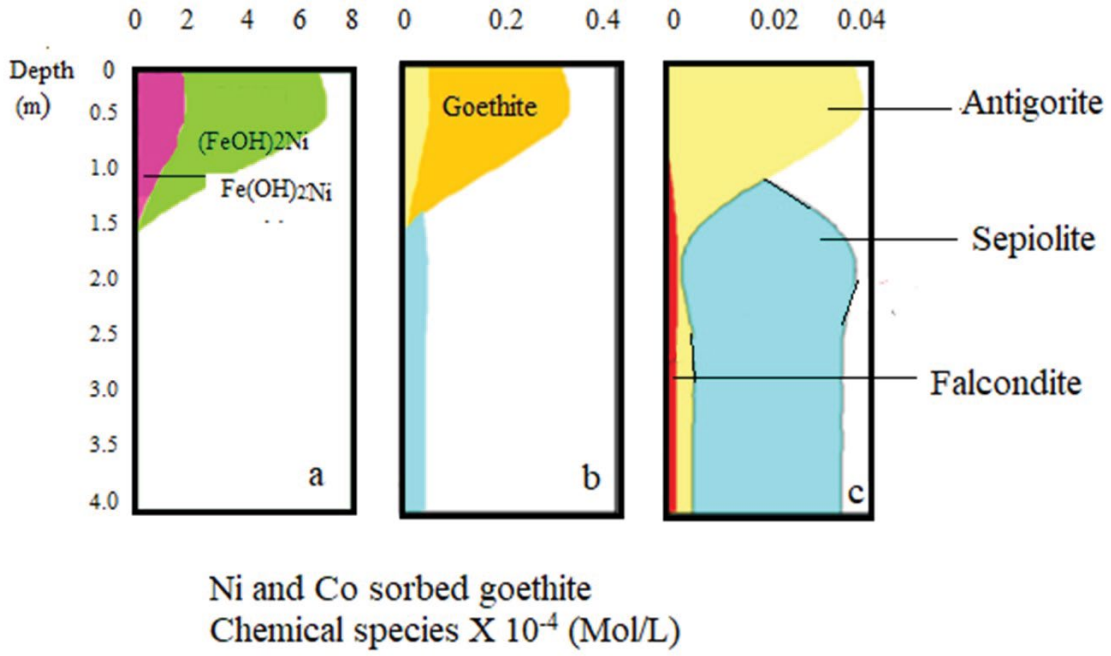

Figure 5: Simulated weathering profile of Falcondo Ni laterite.

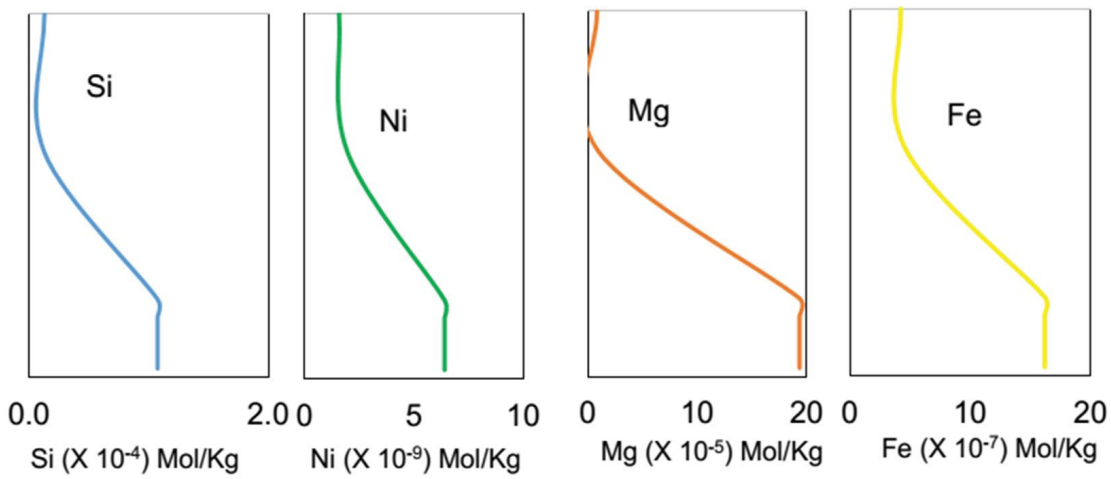

Figure 6: Variation of elements along simulated weathering profile of silicate Ni laterite.

Co, antigorite, goethite, sepiolite, talc, enstatite and Ni_2SiO_4. Herein, the alteration mineral succession depicts that of natural oxic Ni laterite deposits.

The concentration of key elements for different zones of oxide Ni laterite (Figure 8) shows that the amount of Ni and Fe at the limonite zone is directly proportional but their amount decreases at the saprorite zone. This indicates close association between Fe and Ni in goethite in the limonite zone. Silica is zero at the limonite zone but increases rapidly in the saprolite zone. The concentration of Ni varies from 0.003 to 1.18 wt.% from saprolite to limonite zone.

Discussion

These results indicate the presence of a wide-ranging solid solution between Mg and Ni end members. In general, Ni-Mg hydrous silicates from Falcondo and Koniambo Ni lateritehave similar chemical characteristics to garnierite minerals examined in other worldwide Ni-lateritic deposits, excluding the Ni-dominated serpentine-like phases, which have not investigated. It is suggested that Ni mobilization is initiated by fractures which enhances the circulation of water circulation. This process promotes weathering and preferential Ni concentration. There is evidence

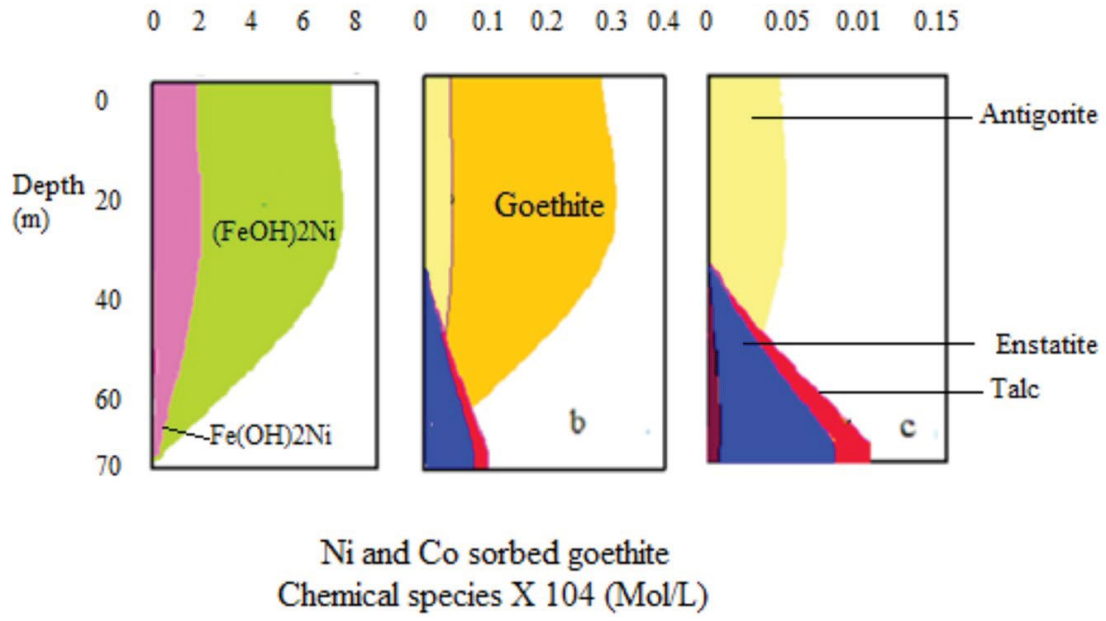

Figure 7: Simulated weathering profile of Koniambo Ni laterite.

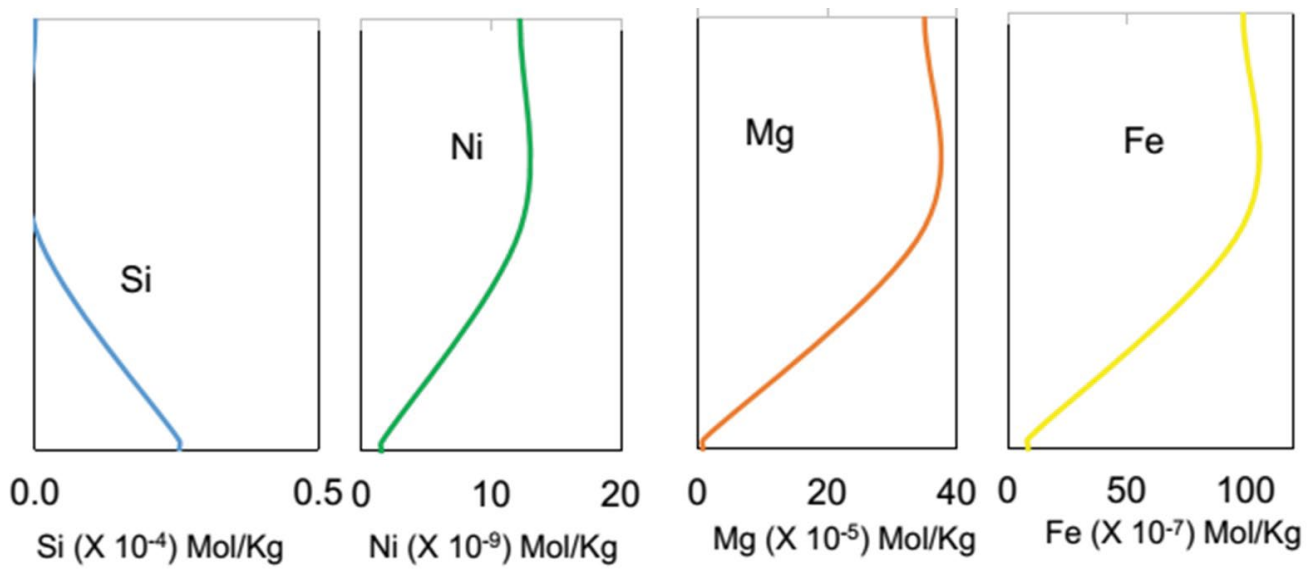

Figure 8: Variation of elements along simulated weathering profile of oxide Ni laterite.

of garnierite precipitation in Falcondo Ni-laterite. Most of garnierite mineralization in the Falcondo mine compose of Ni-sepiolite and falcondoite solid solutions with different concentration [4] which consistent with the simulated Ni laterite (Figure 5). This precipitation is associated with deformation structure that affected the weathering profile [37,38]. The occurrence of these deposits as in fillings and coatings on fracture surfaces, thus precipitating in an energetic dynamic environment. The ultramafic rock suffered uplift before it as altered to several mineral assemblages. This characteristic is indicative of ceaseless dynamic uplift compared to weathering rates. A dynamic environment supported the development of hydrous silicate Ni-laterites, thus promoting cyclic, repeated processes of weathering and denudation. Subsequently, fluids and other reworking migrated at variable depth, remobilized and reconcentrated to form high concentration of Ni ore minerals.

The simulation model of Koniambo Ni laterite indicates the precipitation of silicates at local equilibrium, thus promoting simultaneous precipitation of thermodynamically favorable

minerals. In the end, this pattern induces a narrow zone of Ni precipitation. Naturally, nickel, released due to Ni-Mg hydrous silicates dissolution, is partially lost by crosswise movement in solution. From Figure 4 the migration of transition zone from the limonite horizon to the saprolite, which is marked at 1.5 m and 38 m. The spatial distribution of the mineral phases is consistent with other reports [5,39]. Modelling results indicates that adsorbed nickel is governed by pH front, released into pore water at low pH as since silicates dissolution. It is difficult to explain high nickel content in mineral phases by adsorption alone. In nature, the pH of soil waters is lowered by the presence of dissolved organic acids, thus, it is suggested that nickel concentration is supported by stronger bonding. The stronger bonding is initiated by isomorphous substitution of Ni for Fe in Fe-mineral bearing phases. Surface complexation is useful in understanding metal sorption characteristics at a mineral surface. The simplified version of the complexation model considers a closed system of interaction for Ni and a fixed mineral phase. However, the interaction between Ni-Co and a mineral phase indicates competitive sorption of metals at reactive sites. Subsequent on mineral phase development, adsorption kicks in to regulate the migration of single metal and competitive metals, thus, impeding their migration). Previously, ferrihydrite is considered an initial phase precursor phase in the development of goethite. However, this phase is difficult to identify using standard techniques because of its poor crystallinity. However, the modelling was done using thermodynamic data obtained for ferrihydrite rather than goethite and unable to explain the Ni enrichment in present day laterites.

In summary, modelling the reactive transport simulation of oxide and silicate -type Ni laterite profilesis not limited to pH and depth of Ni laterite but the enormous influence of other cations such as Mg that is released during the alteration of ultramafic rocks. The dissolution process and subsequent competitive sorption are controlled by pH and depth of the profile.

Conclusion

The formation of Ni laterite profile from ultramafic parent rock, at 25 °C, has been simulated by means of PHREEQC one-dimensional reaction-transport code. A reactive transport simulation for the formation of Koniambo Ni laterite, New Caledonia (oxic) and Falcondo Ni (silicate) laterite by weathering of the parent ultramafic rocks at ambient conditions produces a secondary mineral assemblage similar to that observed in the field. The main conclusions are listed below:

1. The descending progression of the pH front controls the mobility of the elements and dictates the Ni enrichment.
2. The precipitation of talc-like silicates at the cost of sepiolite is favoured by high pH due to the dissolution of olivine.
3. The alteration of mineral phases agrees with that of natural Ni laterite deposits.
4. Moreover, the sorption of Co and Ni sorption to goethite involves both surface complexation and irreversible non-ideal structural incorporation.

Hence, application of our surface complexation model to the simulated formation of Co, Ni oxide laterites is only a first-approximation and further refinements of thermodynamic models for the sorption of Co and Ni to goethite are needed.

Acknowledgement

Thanks to Prof Richard Herrington, Natural History Museum, London, Dr Heather Buss and Prof. David Sherman, University of Bristol, United Kingdom for their useful suggestions. This work was supported by the Tertiary Education Trust Fund (TET Fund) of Nigeria.

References

1. Wang J, Zhang Y, Cui K, Fu T, Gao J, et al. (2021) Pyrometallurgical recovery of zinc and valuable metals from electric arc furnace dust - a review. J Clean Prod 298: 126788.
2. Foose MP (1991) Nickel-mineralogy and chemical composition of some nickel-bearing laterites in Southern Oregon and Northern California.
3. Lewis JF, Draper G, Proenza JA, Espaillat J, Jimenez J (2006) Ophiolite-related ultramafic rocks (serpentinites) in the Caribbean region: A review of their occurrence, composition, origin, emplacement and Ni-laterite soil formation. Geologica Acta 4: 237-264.
4. Tauler E, Proenza JA, Gali S, Lewis JF, Labrador M, et al. (2009) Ni-sepiolite-falcondoite in garnierite mineralization from the Falcondo Ni-laterite

deposit, Dominican Republic. Clay Minerals 44: 435-454.

5. Dublet G, Juillot F, Morin G, Fritsch E, Fandeur D, et al. (2012) Ni speciation in a New Caledonian lateritic regolith: A quantitative X-ray absorption spectroscopy investigation. Geochimica et Cosmochimica Acta 95: 119-133.

6. Thorne R, Roberts S, Herrington R (2012) The formation and evolution of the Bitincke nickel laterite deposit, Albania. Mineralium Deposita 47: 933-947.

7. Villanova-de-Benavent C, Proenza JA, Gali S, Garcia-Casco A, Tauler E, et al. (2014) Garnierites and garnierites: Textures, mineralogy and geochemistry of garnierites in the Falcondo Ni-laterite deposit, Dominican Republic. Ore Geology Reviews 58: 91-109.

8. Fu W, Yang J, Yang M, Pang B, Liu X, et al. (2014) Mineralogical and geochemical characteristics of a serpentinite-derived laterite profile from East Sulawesi, Indonesia: Implications for the lateritization process and Ni supergene enrichment in the tropical rainforest. Journal of Asian Earth Sciences 93: 74-88.

9. Soler JM, Lasaga AC (1996) A mass transfer model of bauxite formation. Geochim Cosmochim Acta 60: 4913-4931.

10. Soler JM, Lasaga AC (1998) An advection dispersion reaction model of bauxite formation. Journal of Hydrology 209: 311-330.

11. Lecomte KL, Pasquini AI, Depetris PJ (2005) Mineral weathering in a semiarid mountain river: Its assessment through PHREEQC inverse modelling. Aquatic Geochemistry 11: 173-194.

12. Halim CE, Short SA, Scott JA, Amal R, Low G (2005) Modelling the leaching of Pb, Cd, As, and Cr from cementitious waste using PHREEQC. Journal of Hazardous Materials 125: 45-61.

13. Fletcher RC, Buss HL, Brantley SL (2006) A spheroidal weathering model coupling porewater chemistry to soil thicknesses during steady-state denudation. Earth and Planetary Sciences Letters 244: 444-457.

14. Lebedeva MI, Brantle SL (2017) Weathering and erosion of fractured bedrock systems. Earth Surf Process Landforms 42: 2090-2108.

15. Tiruta-Barna L (2008) Using PHREEQC for modelling and simulation of dynamic leaching tests and scenarios. Journal of Hazardous Materials 157: 525-533.

16. Damuchali AM, Asadollahfardi G, Khodadadi A (2012) Effective Parameter Predictions in Metals Transport from the Zanjan Zinc Mine Tailings using PHREEQC. Mine Water and the Environment 31: 339-343.

17. Domènech C, Galí S, Proenza J, Villanova-De-Benavent C (2014) Reactive transport modelling: The Formation of Ni-laterite Profiles (Punta Gorda, Moa Bay, Cuba) Revista de la sociedadespañola de mineralogía 19.

18. Rempel DM, Dietrich WD (2014) A bottom-up control on fresh-bedrock topography under landscapes. Earth, Atmospheric, and Planetary Sciences 111: 6576-6581.

19. Silva Mario de Freitas, Dimitrakopoulos R (2016) Simulation of weathered profiles coupled with multivariate block-support simulation of the Puma nickel laterite deposit, Brazil. Engineering Geology 215: 108-121.

20. Myagkiy A, Truche L, Cathelineau M, Golfie F (2017) Revealing the conditions of Ni mineralization in the laterite profiles of New Caledonia: insights from reactive geochemical transport modelling. Chemical Geology 466: 274-284.

21. Myagkiy A, Golfier F, Truche L, Cathelineau M (2019) Reactive transport modeling applied to Ni laterite ore deposits in New Caledonia: Role of hydrodynamic factors and geological structures in Nimineralization. Geochemistry, Geophysics, Geosystems 20: 1425-1440.

22. Parkhurst DL, Appelo CAJ (1999) User's guide to PHREEQC (Version 2)-A computer program for speciation, batch-reaction, one-dimensional transport, and inverse geochemical calculations. Water-Resources Investigations Report 99-4259.

23. Ugwu IM, Sherman DM (2017) Irreversibility of sorption of cobalt to goethite (α-FeOOH) and disparities in dissolution of aged synthetic Co-goethite: Implication for Ni laterite ore. Chemical Geology 467: 168-176.

24. Ugwu IM, Sherman DM, Bacon CGD (2019) Sorption of nickel onto goethite (α-FeOOH) and desorption kinetics of aged synthetic Ni-goethite: Implication for Ni laterite ore. Chemical Geology 509: 223-233.

25. Gali S, Soler JM, Proenza JA, Lewis JF, Cama J, et al. (2012) Ni enrichment and stability of Al-free garnierite solid-solutions: A Thermodynamic Approach. Clays and Clay Minerals 60: 121-135.

26. Boily JF, Lutzenkirchen J, Balmes O, Beattie J, Sjoberg S (2001) Modeling proton binding at the goethite

(-FeOOH)-water interface. Colloids and Surfaces A: Physicochemical and Engineering Aspects 179: 11-27.

27. Lithgow EW (1993) Nickel laterites of central Dominican Republic Part I. Mineralogy and ore dressing. In: Reddy RG, Weizenbach RN, The Paul E. Queneau Int. Symposium, Extractive Metallurgy of Copper, Nickel and Cobalt Fundamental Aspects. The Minerals, Metals and Materials Society, Portland, 403-425.

28. Proenza JA, Melgarejo JC, Gervilla F (2003) Comments on the paper "Ochreous laterite: A nickel ore from Punta Gorda, Cuba" by Oliveira et al. Journal of South American Earth Sciences 16: 199-202.

29. Wolery TJ (1979) Calculation of chemical equilibrium between aqueous solution and minerals: The EQ3/6 soft-ware package. Lawrence Livermore National Laboratory, Livermore CA, USA.

30. Reddy BJ, Frost RL, Dickfos MJ (2009) Characterisation of Ni silicate-bearing minerals by UVvis-NIR spectroscopy. Effect of Ni substitution in hydrous Ni-Mg silicates. Spectrochimica Acta 71: 1762-1768.

31. https://horizon.documentation.ird.fr/exl-doc/pleins_textes/pleins_textes_6/Mem_cm/07526.pdf

32. Stoessell RK (1988) 25 °C and 1 atm dissolution experiments of seipiolite and Kerolite. Geochimica et. Cosmochimica Acta 52: 365-374.

33. Cornell RM, Giovanoli R, Schneider W (1992) The effect of nickel on the conversion of amorphous iron(III) hydroxide into more crystalline iron oxides in alkaline media. J Chem Tech Biotechnol 53: 73-79.

34. Dzombak DA, Morel FMM (1990) Surface complexation modeling: Hydrous ferric oxide. John Wiley & Sons.

35. Robineau B, Join JL, Beauvais A, Parisot JC, Savin C (2007) Geoelectrical imaging of a thick regolith developed on ultramafic rocks: groundwater influence. Australian Journal of Earth Sciences 54: 773-781.

36. Gleeson SA, Herrington RJ, Durango J, Velasquez CA, Koll G (2004) The mineralogy and geochemistry of the Cerro Matoso SA Ni laterite deposit, Montelibano, Colombia. Economic Geology 99: 1197-1213.

37. Haldemann EG, Buchan R, Blowes JH, Chandler T (1979) Geology of lateritic nickel deposits, Dominican Republic. Int Laterite Symposium 4: 57-84.

38. Mann P, Draper G, Lewis JF (1991) An overview of the geologic and tectonic evolution of Hispaniola. In: Mann P, Draper G, Lewis JF, Geological and tectonic development of the North American-Caribbean plate boundary in Hispaniola. Geol Soc Am Spec Paper 262: 1-28.

39. Sagapoa CV, Imai A, Watanabe K (2011) Laterization process of ultramafic rocks in Siruka, Solomon Islands. Novel Carbon Resour Sci 3: 32-39.

DOI: 10.35840/2631-5033/1867